ChemCatChem

Research Article
doi.org/10.1002/cctc.202101908

Chemistry Europe
European Chemical Societies Publishing

www.chemcatchem.org

Special Collection

Ru on N-doped Carbon for the Selective Hydrogenolysis of Sugars and Sugar Alcohols

Anna Katharina Beine,[a] Jil Ludovicy,[a] Jiachun Chai,[b] Jan P. Hofmann,[b, c] Christoph Glotzbach,[d] Peter J. C. Hausoul,[a] and Regina Palkovits*[a]

Glycols are accessible via metal-catalyzed hydrogenolysis of sugar alcohols such as xylitol obtained from hemicellulose. Ru-based catalysts are highly active but also catalyze side-reactions such as decarbonylation and deoxygenation. To achieve high selectivity, these reactions need to be suppressed. In our study, we introduce heteroatom doped carbon materials as catalyst supports providing high selectivity. Heteroatom doping with nitrogen and oxygen was achieved by treating activated carbon with HNO_3, NH_3 and H_2 or carbonization of organic precursors. For all N-doped materials a high glycol selectivity of ~80% for sorbitol and xylitol and 44% for xylose and glucose was reached. XPS analysis confirms the presence of different nitrogen species at the carbon surface and varying ligand effects for oxygen and nitrogen. Oxygen has an electron withdrawing effect on ruthenium and leads to a decreased activity. Nitrogen has weaker electron withdrawing properties, resulting in an enhanced selectivity.

Introduction

The use of lignocellulosic biomass as feedstock for renewable commodity and fine chemicals reduces CO_2 emissions and mitigates the dependence on fossil resources. The production of glycols, used as monomers in the chemical industry, offers the possibility to substitute fossil by renewable raw materials.[1–2] Sugar alcohols such as the hemicellulose derived platform molecule xylitol (XYL) can be used as feedstock.[3] The conversion to ethylene and propylene glycol (EG and PG) involves many reaction mechanisms such as metal catalyzed dehydrogenation and hydrogenation or base promoted retro-aldol splitting (Scheme 1).[4–7] Glycerol (GLY) is formed in significant amounts as by-product as well as the side product lactic acid (LA). In addition, side-reactions like decarbonylation and deoxygenation can degrade the formed products. As a result, a wide range of products is obtained. To enhance selectivity, many monometallic catalysts based on Cu, Ni, Pt or Ru were developed and tested in combination with a homogeneous base.[8–14] Additionally, recent research focused on the development of bimetallic catalysts to facilitate reactions with the addition of a solid base, without external hydrogen pressure or to further enhance selectivity.[15–24]

Nevertheless, selectivity and activity control remains a major challenge.[25] In particular, ruthenium catalyzes side-reactions which lead to the formation of C_1-products.[6,26] Nonetheless, it is a highly interesting active metal for hydrogenolysis reactions due to its relatively low price, good corrosion resistance and high activity. A work by Sun *et al.* on the influence of the catalyst support for Ru revealed activated carbon (AC) to be the most selective support in hydrogenolysis reactions.[8] AC is chemically inert, resistant to basic and acidic medium and provides high surface areas.[27] For Ru/C, 57% glycol selectivity was observed at low XYL conversion of 20%. The selectivity drops over time due to side-reactions.[28] After 4 h under the same conditions only 35% glycol selectivity could be obtained.

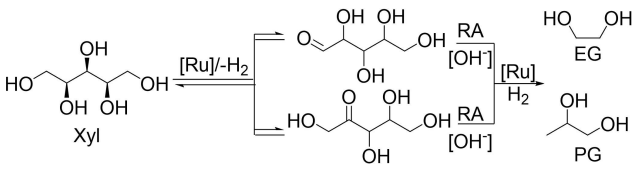

Scheme 1. Conversion of xylitol to glycols via dehydrogenation, retro-aldol splitting and hydrogenation.

[a] Dr. A. K. Beine, J. Ludovicy, Dr. P. J. C. Hausoul, Prof. R. Palkovits
Institute of Technical and Macromolecular Chemistry
RWTH Aachen University
Worringer Weg 2, 52074 Aachen (Germany)
E-mail: palkovits@itmc-rwth-aachen.de
[b] J. Chai, Prof. J. P. Hofmann
Laboratory for Inorganic Materials and Catalysis
Department of Chemical Engineering and Chemistry
Eindhoven University of Technology
Postbox 513
5600MB Eindhoven (The Netherlands)
[c] Prof. J. P. Hofmann
Surface Science Laboratory
Technical University of Darmstadt
Otto-Berndt-Strasse 3
64287 Darmstadt (Germany)
[d] C. Glotzbach
thyssenkrupp Industrial Solutions AG
Friedrich-Uhde-Straße 15
44141 Dortmund (Germany)

Supporting information for this article is available on the WWW under https://doi.org/10.1002/cctc.202101908

This publication is part of a Special Collection on "55. Jahrestreffen Deutscher Katalytiker". Please check the ChemCatChem homepage for more articles in the collection.

As a result, different strategies to enhance the selectivity of the catalysts were explored: e.g. promotion with basic metal oxides,[29–31] bimetallic catalysts[32] and variation of carbon-based supports.[33–34] Rivière *et al.* promoted the Ru/C catalyst with basic metal oxides performing reactions without the use of a homogenous base.[29] The best catalyst Ru/MnO/C only reached a glycol selectivity of 22% in XYL hydrogenolysis and suffered from leaching of the metal oxides due to LA formation. The same group also demonstrated that using a solvent mixture of water and primary alcohol (90:10 v/v) improves selectivity to 70%.[30] However, catalyst deactivated during reaction due to coke formation coke formation. RuRe/C catalysts developed by Jin *et al.* provided higher amounts of liquid phase products, yet glycols were only formed with a selectivity of 23%.[32] The observed effect was attributed to the modification of the electronic structure of Ru by alloy formation. Zhao *et al.* reported a yield of 20% EG and 38% PG, using carbon nanofibers (CNF) as support.[33] Guo *et al.* compared AC and carbon nanotubes (CNT) and found a higher activity for Ru/CNT in the hydrogenolysis of sorbitol (SOR). The difference was attributed to the higher degree of graphitization for CNT and improved electronic interactions between the support and the metal.[34] Promoting the Ru/CNT catalyst with WO_x led to an even higher glycol selectivity of 60%. The physical mixture of Ru/CNT and W/CNT was also able to catalyze EG formation from cellulose with a high yield of 51% and moderate activity.[31]

Additionally, the doping of carbon supports with heteroatoms was studied. The use of a sulfur modified Ru/C catalyst led to a high glycol selectivity of 68% for XYL, whereas the catalyst was four times less active than undoped Ru/C.[35] Tronci *et al.* observed an increased selectivity of 41% to PG and 26% to EG for a comparable catalyst in the hydrogenolysis of SOR. However, the activity decreased significantly so that only 14% conversion was reached after 4 h, indicating catalyst inhibition.[36] Guo *et al.* investigated the influence of functional groups for CNT.[37] Ru/CNT-NH_2 provided the highest selectivity of 35% to PG and 24% to EG at 27% SOR conversion. Jin *et al.* investigated bimetallic PtPd catalysts supported on N-doped mesoporous carbons in the base-free hydrogenolysis of SOR.[19] The heteroatom functions as Lewis base as well as a lattice manipulator adjusting the electronic properties of the bimetallic nanoparticles. Previously, we reported that the use of covalent triazine frameworks (CTF) as N-containing supports for Ru leads to a high selectivity of 80% to glycols and to the suppression of decarbonylation reactions.[28] The improved performance was attributed to the presence of nitrogen in the support, which donates electrons to the active metal and influences the Ru surface chemistry.

CTF materials became rather prominent after Kuhn *et al.* published a relatively easy preparation method using ionothermal synthesis.[38] Since then they have been widely used in gas adsorption, as electrode materials, catalysts and catalyst supports.[39–44] These materials possess high specific surface areas and N-contents, however the used monomers are rather expensive, the procedure is very water intensive and not easily scalable. When considering a potential process for the hydrogenolysis of sugars and sugar alcohols, cheaper support materials with a scalable synthesis are required. In literature, many N-doped carbon materials have been presented for use as electrodes or in gas or water adsorption, but rarely in catalysis.[45–50] Herein, we present a systematic study on N-doped carbon materials as supports for Ru-catalysts in the hydrogenolysis of XYL in the presence of $Ca(OH)_2$. Various N-doping methods were explored and the resulting materials characterized. In addition, the influence of O-doping was studied to differentiate between the electronic effects of oxygen and nitrogen on Ru.

Results and Discussion

Synthesis and Characterization

To produce a wide spectrum of O- and N-doped carbon materials, three different synthesis strategies were applied, and the performance of the Ru-loaded catalysts was compared to an untreated Ru/AC catalyst. In the first N-doping method (M1), AC was ground together with cyanamide (C) or melamine (M) and carbonized under N_2-atmosphere, yielding the amorphous carbon materials AC–C and AC–M (Table1, entries 3–5). In the second method (M2), AC was treated with gaseous NH_3 at different temperatures *T* for a reaction time *t* of 1 h or 5 h and denoted N–*T*,*t* (Table 1, entries 6–10). In the third method (M3), AC was treated in refluxing HNO_3 (AC–HNO_3) (Table 1, entry 11) and additionally reduced by ammonia (AC–HNO_3/NH_3) and then hydrogen (AC–HNO_3/NH_3/H_2) (entries 12–13). The prepared materials were characterized by N_2-Physisorption, TGA (in air) and elemental analysis. All N_2-physisorption isotherms of the prepared supports are of type I (IUPAC) corresponding to microporous materials and are depicted in Figure S1 in the electronic supplementary information (ESI). The elemental analysis data are given in Table S1 in the ESI. All prepared materials are highly stable in air and show decomposition temperatures of over 830 K (Figure S2 in the ESI). The parent AC possesses a negligible N-content of 0.2%, an O-content of 6.8%, a specific surface area (S_{BET}) of 1784 m^2/g and a total pore volume (*PV*) of 0.93 cm^3/g (Table 1, entries 1–2). The AC was loaded with 5 wt% Ru using wet impregnation (i.e. all the introduced Ru is loaded onto the support by complete evaporation of the solvent). By applying equilibrium-impregnation (i.e. after coordination the catalyst is filtered off and washed), a loading of 1.5 wt% could be realized. After M1, S_{BET} and *PV* are slightly decreased and TGA analysis confirms the absence of any remaining organic precursors. The N-content of the materials AC–C and AC–M increased to 2.6% and 2.4%, respectively. The O-content changed only slightly. The materials were loaded with 1 or 5 wt% Ru using wet-impregnation. TEM analysis of the reduced 1 wt%- and 5 wt%-loaded AC–C reveals the formation of small nanoparticles with narrow particle size distribution (Figure 1a–d). 1%Ru/AC–C shows an average particle size of 1.3 nm whereas for 5%Ru/AC–C the particle size distribution is shifted to larger particles with a mean size of 1.8 nm. EDX analysis confirms the visible particles to be Ru (Figure S3 in the ESI). For M2, S_{BET}, *PV* and N-content increased

Table 1. Specific surface area (S_{BET}), total pore volume (*PV*), N- and O-content as well as Ru-loading.

#	Method	C-support	S_{BET} [m^2/g]	*PV* [cm^3/g]	N-content [%]	O-content [%]	Ru-loading [%]
1		AC	1784	0.93	0.2	6.8	1.5[a]
2							5.0[b]
3	M1	AC–C	1682	0.83	2.6	7.2	1.0[b]
4							5.0[b]
5		AC–M	1706	0.84	2.4	6.5	1.0[b]
6	M2	N-873/1	1584	0.80	0.5	4.4	4.4[a]
7		N-873/5	1807	0.92	0.6	4.5	4.8[a]
8		N-1073/1	1783	0.92	1.5	4.6	3.4[a]
9		N-1073/5	1983	1.02	1.6	5.8	3.4[a]
10		N-1173/1	1949	1.02	1.2	5.9	1.4[a]
11	M3	AC–HNO_3	1318	0.68	1.3	13.7	1.4[a]
12		AC–HNO_3/NH_3	1344	0.75	4.0	8.7	4.8[a]
13		AC–HNO_3/NH_3/H_2	1277	0.71	4.2	7.7	3.9[a]

[a] Equilibrium-impregnation (ICP-MS); [b] Wet-impregnation.

with increasing temperature and reduction time accompanied by a loss of mass. A maximum N-content of 1.6% was obtained for N-1073/5. Due to the reductive treatment, the O-content of all materials decreased by 1.9 to 2.4% compared to the parent AC. Equilibrium-impregnation yielded varying loadings of up to 4.8 wt% Ru for N-873/5. Supposedly, the metal only coordinates to the heteroatoms in the support, however, no clear trend between metal loading and N- or O-content could be observed. After reduction a narrow particle size distribution and a mean particle size of 1.3 nm is found for N-1173/1 (Figure 1e and f). M3 introduced 13.7% oxygen and 1.3% nitrogen (AC–HNO_3). Further treatment with ammonia (AC–HNO_3/NH_3) led to an increased N-content of 4.0%, while the O-content decreases to 8.7% (Table 1, entry 12). A subsequent treatment with H_2 (AC–HNO_3/NH_3/H_2), kept the N-content at 4.2% while further decreasing the O-content to 7.7% (Table 1, entry 13). For all HNO_3 treated AC materials an approximately 500 m^2/g decreased specific surface area and lower pore volume compared to AC was found. The materials were loaded using equilibrium-impregnation. Ru-loadings between 1.4 wt% and 4.8 wt% were obtained, which did not correlate to the amount of heteroatoms. TEM-analysis confirms the formation of highly dispersed nanoparticles with an average particle size of 1.8 nm (Figure 1g and h).

Catalyst Screening

Ru-catalyzed hydrogenolysis of XYL was carried out at 473 K under 8.0 MPa H_2 pressure and in the presence of $Ca(OH)_2$. XYL in the following describes the sum of all C_5-sugar alcohols (xylitol, ribitol and arabitol). For all catalysts EG, PG, GLY and LA are formed in the liquid phase. In order to evaluate catalyst selectivity, all reactions are compared at similar conversion with the exception of the 1 wt% loaded M1-catalysts, which show a slower conversion due to the lower amount of active metal used in the reaction. Ru/AC (catalyst #1) yields a combined glycol selectivity (sum of EG and PG) of 61% after 4 h (Figure 2). 5%Ru/AC (catalyst #2) instead needs only a reaction time of 1 h to reach a conversion of 91% even though the same amount of active metal was used in the catalysis. The development of conversion over time for both AC-based catalysts is depicted in Figure S4 in the ESI. The Ru-particles on the 5 wt% loaded catalyst are thus more active when compared to the catalyst prepared by equilibrium-impregnation. As AC contains oxygen as heteroatom, it is likely that the metal coordinates to these moieties by equilibrium-impregnation. For the catalyst prepared by wet-impregnation, it is likely that also coordination to amorphous carbon occurs by Van der Waals forces. The coordination to oxygen thus influences ruthenium and decreases its catalytic activity. The selectivity to glycols sums up to 58% and is comparable for both AC-catalysts. Therefore, the interaction with oxygen seems to influence only activity but not selectivity. The mass balance decreases with time due to the formation of gaseous products such as CH_4 and CO_2 (the development of the selectivity over time is exemplarily depicted for 5%Ru/AC in Figure S5 in the ESI).[28]

5%Ru/AC–C shows a comparable glycol selectivity of 57% and a non-closed carbon balance after 4 h. If the reaction is carried out for 0.5 h, the carbon balance can be closed but still the selectivity to glycols is low with 63%. Lowering the catalyst loading to 1 wt% instead leads to an increased selectivity of 83% at comparable conversion. Also for 1%Ru/AC–M, a selectivity of 78% is reached. For both catalysts, the carbon balance is closed and no side-reactions occur. As for both 1 wt% and 5 wt% Ru/AC–C small Ru nanoparticles below 2 nm are formed, the observed differences in selectivity rather result from changes in the electronic structure of the active metal than from dispersion. As it is known from our previous study, the coordination of Ru to nitrogen leads to a higher glycol selectivity and decreased decarbonylation activity.[28] Due to the high metal loading of 5 wt% Ru/AC–C, the influence of nitrogen decreases as particles might also interact with the amorphous carbon. As a result, a comparable selectivity as for the Ru/AC catalysts is reached. In order to ensure a high glycol selectivity using Ru on N-doped carbon materials, it is therefore essential to load the catalyst with only as much Ru as the heteroatoms on the catalyst surface can bind.

Catalysts prepared by method M2 and M3 were thus only loaded by using equilibrium-impregnation. A high glycol

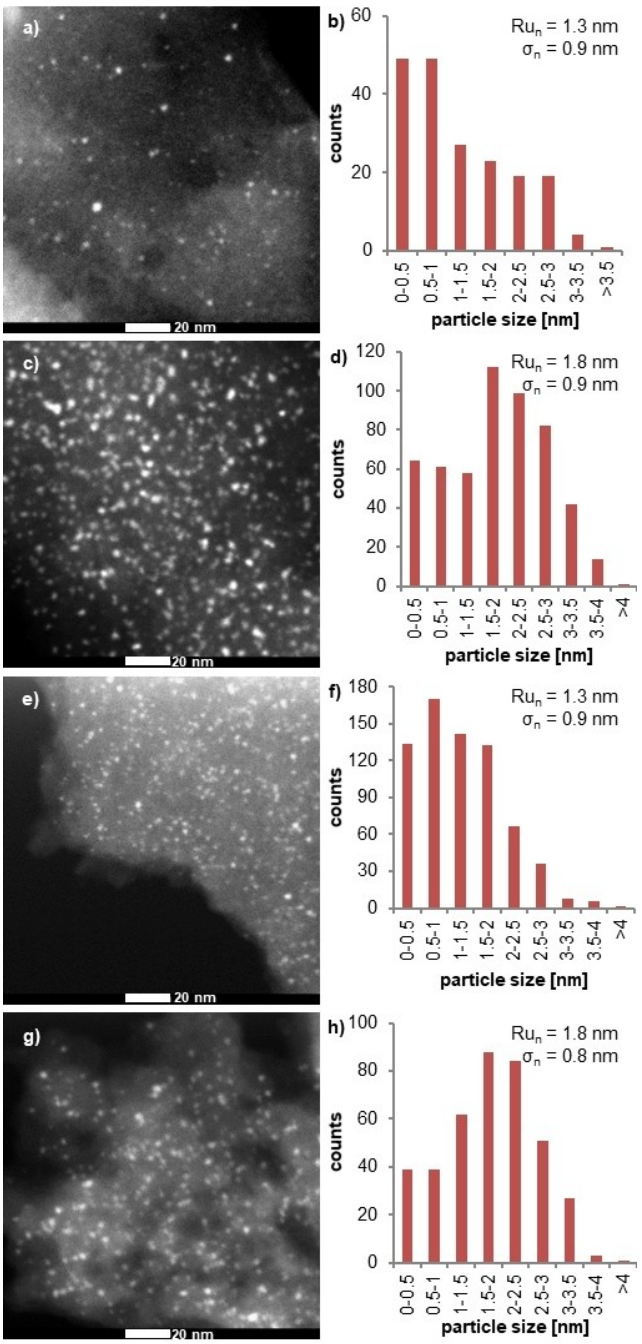

Figure 1. Dark field TEM-images and particle size distributions for 1wt%Ru/AC–C (a, b), 5wt%Ru/AC–C (c, d), Ru/N-1173/1 (e, f), Ru/AC–HNO3/NH3 (g, h).

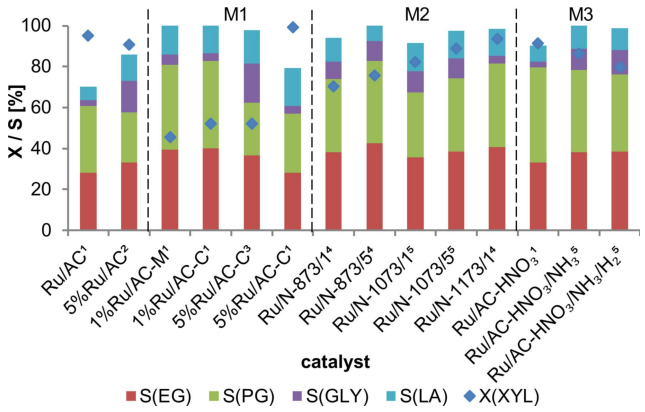

Figure 2. Comparison of prepared catalysts in the hydrogenolysis of XYL in terms of selectivity (conditions: 473 K, 8.0 MPa H_2, 1) 4 h, 2) 1 h, 3) 0.5 h, 4) 3 h, 5) 2 h, 2.0 g XYL, 10 mg Ru (for M1: 0.2 g catalyst), 0.3 g $Ca(OH)_2$, 20 mL H_2O).

selectivity of up to 83% is reached for all M2 support materials. With increasing reduction time of the support, a slightly increasing selectivity is observed. Materials prepared using M3 possess a high N-content of up to 4.22%. Additionally, an increased O-content is observed. Nevertheless, all catalysts facilitate a high glycol selectivity between 76 and 80%. If the activity of the Ru/M3 catalysts is compared (see Figure S6 in the ESI), a decreased activity is observed for Ru/AC–HNO_3 even though the same amount of active metal was used. As this support material possesses the highest O-content among all synthesized materials, the inhibiting effect of oxygen on activity is monitored again.

The stability of the catalysts was exemplarily investigated using Ru/N-873/1 as catalyst (Figure S7 in the ESI). Four consecutive recycling runs were performed, where conversion decreased slightly from 99% to 91% indicating a minor decrease of activity. A constant selectivity of ~66% was observed throughout the recycling. Leaching of Ru into the liquid phase was investigated by ICP-MS and found to be below 0.0001% for all reactions. From the results, it can be concluded that doping of AC with nitrogen increases the catalysts selectivity to the desired glycols. Oxygen doping on the other hand decreases the catalytic activity without influencing selectivity. The effects of O- and N-doping therefore need to be investigated in more detail.

Role of the Heteroatom

To elucidate the influence of nitrogen and oxygen on the active metal, the two carbon materials AC and AC–HNO_3 as well as the Ru-loaded carbons were investigated by X-ray photoelectron spectroscopy. From the survey spectrum of the parent AC it is apparent that the catalyst surface mainly consists of carbon and oxygen, nitrogen is not detected (Figure S8 a and b in the ESI). The C 1s spectrum was fitted by using seven different carbon species (Figure 3a).[51–52] These species can be assigned to sp^2-hybridized (C=C, 284.5 eV) and sp^3-hydbridized carbon (C–C, 285.0 eV). Additionally, carbon species bound to oxygen can be identified such as ether (C–O–C, 286.5 eV), carbonyl (C=O, 288.0 eV) and carboxyl groups (O–C=O, 289.0 eV). The two additional signals at 290.1 eV and 291.3 eV correspond to π–π* shake-up satellite transitions typically observed for graphitic carbon materials.[52] For AC–HNO_3 the ratio of O/C on the surface increases from $5.2\cdot10^{-2}$ (AC) to $13.0\cdot10^{-2}$ and nitrogen is introduced with a ratio of N/C of $1.2\cdot10^{-2}$ (Figure S8 c in the ESI). The C 1s signal indicates an increased amount of

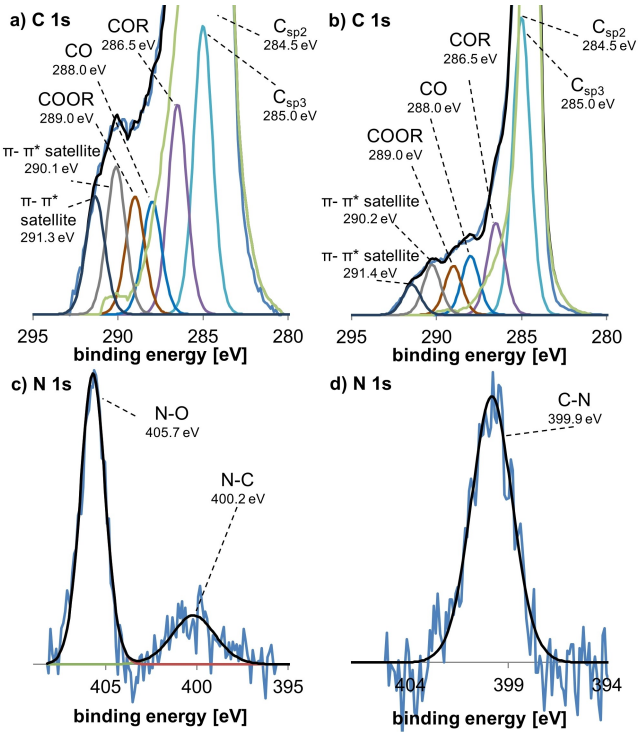

Figure 3. XPS C1s spectra of AC (a), AC–HNO_3 (b) as well as N 1s spectra of AC–HNO_3 (c), reduced Ru/AC–HNO_3 (d).

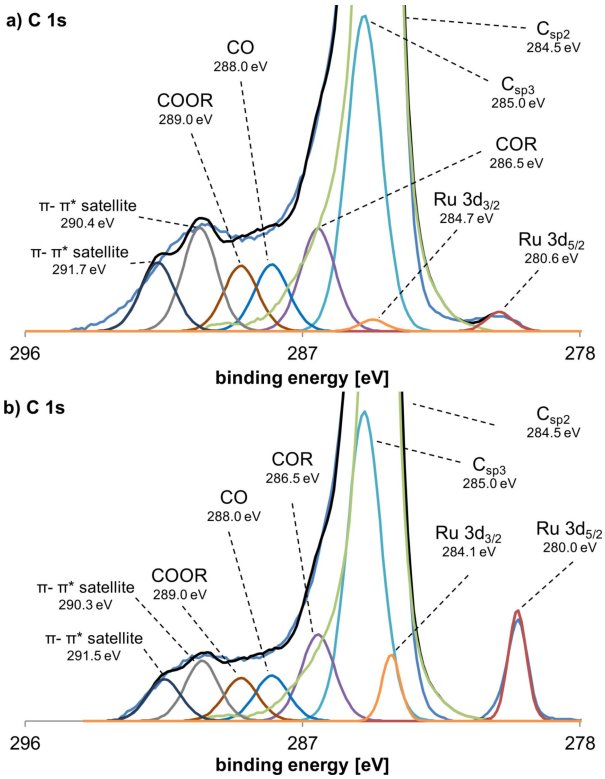

Figure 4. XPS C 1s spectra of the reduced Ru/AC (a) and Ru/AC–HNO_3 (b) catalysts.

sp^3-hybridized carbon on the surface, implying that the acid treatment creates defects in the aromatic carbon structure decreasing the degree of graphitization (Figure 3b). In the N 1s region, two signals occur which are assigned to N–O species such as in nitro or nitroso groups (405.7 eV)[53] and N–C species such as pyridinic, pyrollic and graphitic nitrogen (400.2 eV) (Figure 3c).[28]

AC and AC–HNO_3 were afterwards impregnated with $[RuCl_2(p-cymene)]_2$ by equilibrium impregnation. The Ru-loaded samples were reduced in H_2 atmosphere at 623 K in a high-pressure treatment chamber connected to the spectrometer, directly transferred *in vacuo* to the analysis chamber and measured by XPS (Figure 3d and 4). The O/C ratio decreases for both samples upon loading and reductive treatment (Figure S9 in the ESI). For Ru/AC and Ru/AC–HNO_3 an O/C ratio of $0.8 \cdot 10^{-2}$ and $5.6 \cdot 10^{-2}$ is obtained, respectively. Additionally a decreased N/C ratio of $0.6 \cdot 10^{-2}$ is observed for Ru/AC–HNO_3. In the N 1s spectrum, the N–O signal disappears, and only N–C species are observed (399.9 eV) (Figure 3d). These changes in the surface composition can either result from the active metal coordinating to nitrogen and oxygen or from the reductive treatment. Since the metal loading is low, it appears likely that reduction is the most plausible explanation.

The Ru 3d components in Ru/AC and Ru/AC–HNO_3 were fitted by a spin-orbit split doublet with a separation of 4.1 eV. The Ru $3d_{5/2}$ signal appears for Ru/AC at a binding energy of 280.6 eV indicating a reduced oxidation state of Ru (Figure 4a).[53] For Ru/AC–HNO_3, the Ru $3d_{5/2}$ signal is shifted by −0.6 eV to lower binding energies to a value of 280.0 eV (Figure 4b). A comparable result was already found for Ru/CTF catalysts in our previous study, where the lower binding energy for Ru/CTF compared to Ru/C resulted from ruthenium bonding to nitrogen in the support.[28] Even though both reduced catalysts confirm the presence of metallic Ru on the surface, an increased Ru 3d binding energy is found for O-containing supports compared to N-containing supports. The presence of oxygen seems to have an electron withdrawing effect reducing the electron density at the Ru metal center, which results in a decreased activity in the hydrogenolysis reaction. If nitrogen functionalities (such as pyridinic, pyrollic and graphitic nitrogen) are introduced, a less electron withdrawing effect is observed, enhancing the selectivity. Which of the mentioned N-species exactly serves as coordination site for Ru and what the electronic effects of each species are cannot be clarified within the scope of this study. The detailed understanding of the role of the different N-species thus requires further study. As the shift in binding energy already occurs for a support with low N-content and high O-content (1.3 wt% N and 13.3 wt% O, see Table 1, entry 11), nitrogen seems to be preferred over oxygen as coordination site. From these results, it becomes evident, that doping of carbon with oxygen and nitrogen results in different ligand effects in combination with the active metal Ru and hence to an alteration of selectivity towards EG and PG.

Hydrogenolysis of Sugar Alcohols and Sugars

To further investigate the suitability of the prepared carbon materials for an industrial biomass conversion process, the substrate scope was expanded to SOR (Figure S10 in the ESI). Ru/AC–HNO_3 was used as catalyst. After 2 h of reaction a conversion of 25% of SOR was reached and EG and PG were formed with a selectivity of 25% and 61%, respectively. For an economically feasible process next to a cheap catalyst, also the reduction of reaction steps is important. Therefore, the direct conversion of the sugars xylose and glucose was investigated using Ru/N-873/5 as catalyst. To realize hydrogenation and hydrogenolysis in a one-pot reaction, a two stage-process was applied. First, the autoclave was heated to 373 K for one hour for hydrogenation. Afterwards the temperature was increased to 473 K for another hour to enable hydrogenolysis (Scheme 2).

For both sugars, a conversion of over 90% is reached (Figure 5). In the reaction glycols are formed with a combined selectivity of 45% and 44% for xylose and glucose, respectively. Additionally, LA and GLY are formed with a selectivity of 25% to 26%. Next to these products also the corresponding sugar alcohols XYL or SOR are formed with a selectivity of 10% and 13%, respectively. For both reactions the carbon balance in the liquid phase lies between 80% and 83%. The gap in the balance suggests the formation of gaseous products by, for example, decarbonylation. In addition, the formation of soluble and insoluble polymers of the reactive sugars is possible, which is evident from the yellowish-brown coloration of the reaction solution. The data clearly emphasize the potential of N-doped carbon materials to not only provide an efficient access to EG and PG but also to realize a one-pot approach to glycols starting directly from sugars.

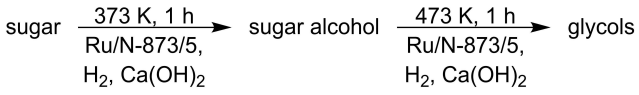

Scheme 2. Conversion of sugars over Ru/N-doped carbon using a two-stage one-pot reaction.

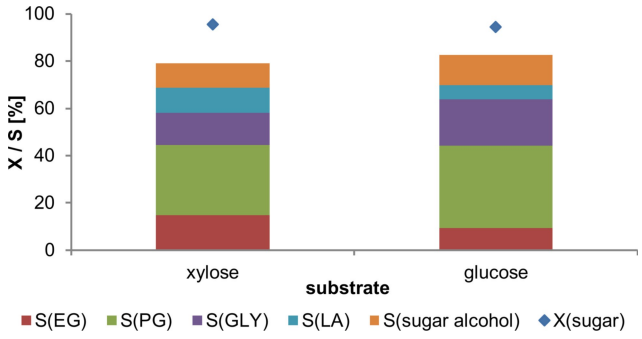

Figure 5. Conversion and selectivity in the hydrogenolysis of sugars using Ru/N-873/5 (conditions: 373–473 K, 8.0 MPa H_2, 2 h, 6.24 mmol sugar, 4.8 mg Ru, 72 mg $Ca(OH)_2$, 9.6 mL H_2O).

Conclusion

In our study, we have shown that N-doped carbon materials can successfully function as catalyst support for Ru in the hydrogenolysis of sugars and sugar alcohols. Different N-containing carbon materials were synthesized by treating AC with NH_3, HNO_3 and H_2 or by carbonization of AC with organic precursors. The different synthesis procedures result in materials with high specific surface area of over 1270 m^2/g and high N-content of up to 4.22%. In addition, the O-content of the carbon supports was affected by the different chemical treatments. Loading with Ru yielded catalysts that possess small nanoparticles with an average particle size below 2 nm for all preparation methods. To reach high glycol selectivity, the metal loading proved to be highly important. When the impregnation proceeds *via* equilibrium-impregnation, high glycol selectivity and the suppression of decarbonylation side-reactions can be ensured for all materials independent of preparation method, N-content and the presence of oxygen. For XYL, a maximum selectivity to EG and PG of 83% was reached. In contrast, the Ru-loaded O-containing AC, which is used as starting material for the synthesis of all catalyst supports, only provides a low glycol selectivity of around 60%. Coordination of the active metal Ru to oxygen was found to decrease catalytic activity but had no positive impact on selectivity. XPS analysis confirmed that the active metal is electronically affected by nitrogen and oxygen. For oxygen an electron withdrawing effect is found, which is less pronounced for nitrogen. This leads to a shift of the Ru 3d binding energy by −0.6 eV for Ru/AC–HNO_3 compared to Ru/AC. In addition, hydrogenolysis of glucose and xylose in one-step could be demonstrated yielding glycols with at least 44% selectivity. All in all, the hydrogenolysis of sugars and sugar alcohols over Ru-based catalysts can be optimized by using N-doped carbon as catalyst support.

Experimental Section

Chemicals

If not stated otherwise chemicals were used as delivered. Chemicals were purchased from Acros Organics (AC Norit A Supra), Alfa Aesar (Cyanamide), Gerling Holz & Co. (NH_3), Merck ($Ca(OH)_2$, D-Glucose), ROTH (HNO_3, D-Xylitol), Sigma Aldrich (Melamin, $[RuCl_2(p\text{-Cymene})]_2$, D-Sorbitol, D-Xylose) and Westfalen (H_2).

Analytical Methods

The catalysts and supports were analyzed by N_2-physisorption (Quadrasorb SI by Quantachrome Instruments). Materials were degassed in a FloVac Degasser by Quantachrome Instruments in vacuum at 393 K for at least 4 h prior to measurement. Transmission electron microscopy (TEM) was performed on a Tecnai G2 F20 S-TWIN. Prior to measurement the materials were reduced in a tube furnace under a H_2 flow of 6 L/h for 3 h at 623 K. Thermogravimetric analysis (TGA) was performed in air with heating rate of 5 K/min in a STA 409 cell by Netzsch. The elemental composition was obtained using a 2400 CHNS/O Series II System by PerkinElmer. Prior to the measurement the samples were dried in vacuum at 333 K for 24 h and handled under Ar-atmosphere to

ensure a reliable N-content. Every sample was measured twice. X-ray photoelectron spectroscopy (XPS) was performed on a Thermo Scientific K-Alpha spectrometer equipped with a monochromatic small-spot X-ray source and a 180° double focusing hemispherical analyzer with a 128-channel delay line detector. *Quasi in situ* X-ray photoelectron Spectroscopy (XPS) was performed in a Kratos AXIS Ultra 600 spectrometer equipped with a monochromatic Al K_α X-ray source ($h\nu = 1486.6$ eV). Survey scans were measured at constant pass energy of 160 eV (step size 0.5 eV) and high-resolution scans of the separate regions were measured at a pass energy of 40 eV (step size 0.1 eV) with the background pressure kept below 5×10^{-9} mbar. A high-temperature reaction cell (Kratos, WX-530) was used to pretreat the Ru-loaded sample, which was mounted on a stainless-steel stub. This allowed *in vacuo* sample transfer into the XPS analysis chamber. Samples were reduced at atmospheric pressure under a H_2 flow of 6 L/h for 7 h at 623 K. The sample was transferred from the reaction cell to the XPS analysis chamber after reduction and evacuation *in vacuo*, i.e. without exposure to ambient conditions to avoid re-oxidation. Binding energy calibration was performed by setting the C1s peak of graphitic sp^2 carbon to 284.5 eV. Data treatment and fitting was performed using the software CasaXPS (version 2.3.24). Organic and aqueous liquid samples of catalyst preparation and catalysis were analyzed by ICP-MS and HPLC. ICP-MS analysis was performed on an 8800 ICP-MS Triple Quad device by Agilent. HPLC analysis was performed on a Shimadzu system (Rezex ROA Organic Acid H^+ (8%) column by Phenomenex, eluent: 0.05 M H_2SO_4).

Preparation of N- and O-doped Carbon

Carbonization with organic precursors (M1)

Doping of AC using melamine was performed based on the procedure of Le *et al.*[45] 1.0 g of AC and 10.0 g of melamine were ground together until a homogeneous sample was obtained. Doping of AC using cyanamide was performed based on the procedure of Zhang *et al.*[46] 1.5 g of AC and 7.5 g of cyanamide were ground together until a homogeneous sample was obtained. The samples were dried at 153 K for 1 h. Afterwards, the temperature was increased to 1073 K applying a heating rate of 3 K/min and maintained for 2 h. Carbonization was performed under a N_2-flow of 6 L/h. The materials are named AC–C for cyanamide and AC–M for melamine.

Ammonia reduced carbon (M2)

AC was reduced with NH_3 in a tube furnace at a given temperature (T = 873/1073/1173 K) for a given time (t = 1/5 h). The gas flow was regulated to 6 L/h. During heating and cooling the furnace was flushed with N_2. The materials are named N–T/t (e.g. the materials N-873/5 was reduced with ammonia at 873 K for 5 h).

HNO_3 treated carbon (M3)

5 g AC were treated with HNO_3 (30%) under reflux for 8 h. The resulting carbon material was then washed neutral and dried at 393 K to obtain the material AC–HNO_3. 1 g of AC–HNO_3 was then reduced with NH_3 in a 50 mL stainless steel autoclave by applying 0.8 MPa NH_3 and 5.2 MPa of N_2. Reduction took place at 473 K for 4 h to obtain AC–HNO_3/NH_3. The material was afterwards reduced in a tube furnace at 623 K for 7 h under a H_2-flow of 6 L/h. The resulting material is denoted AC–HNO_3/NH_3/H_2.

Impregnation of the support

Typically, metal salt ($[RuCl_2(p-cymene)]_2$ (106 mg, 0.173 mmol) and support (700 mg) were dispersed in ethanol (200 mL). The suspension was refluxed for 48 h under inert gas atmosphere. In case of wet-impregnation, the solvent was afterwards removed under vacuum and the catalyst was dried at 373 K in an oven overnight. For equilibrium-impregnation, the catalyst was filtered, washed with ethanol (60 mL) and dried under vacuum at 333 K. The filtrate was concentrated in vacuum, the residue dissolved in ethanol (10 mL) and analyzed by ICP-MS to calculate the obtained catalyst loading.

Catalytic tests

Hydrogenolysis reactions were carried out in a 50 mL stainless steel autoclave equipped with a Teflon inlet and a sampling tube. All reactions were performed at 473 K while stirring with a magnetic stirrer at 750 rpm. In a typical experiment, the autoclave was charged with XYL (2.00 g, 13.1 mmol, 1 eq.), catalyst (m(Ru) = 10 mg), $Ca(OH)_2$ (0.3 g, 4.0 mmol OH^-, 0.3 eq.) and water (deionized, 20 mL). The autoclave was flushed 3 times and pressurized with 8.0 MPa H_2. Samples were taken periodically and filtered over a syringe filter (Chromafil®PA 45/25). For catalyst recycling, the reaction solution with catalyst was centrifuged and the supernatant was removed. The wet catalyst was washed three times with water and used in the next reaction without further drying.

Acknowledgements

We thank Noah Avraham, Simon Petring, Julia Nießen and Kalle Vaeßen for HPLC, ICP-MS and TGA analyses. Part of this work was supported by the German federal ministry of education and research (BMBF) under grant number FKZ 031B0667. Open Access funding enabled and organized by Projekt DEAL.

Conflict of Interest

The authors declare no conflict of interest.

Data Availability Statement

The data that support the findings of this study are available from the corresponding author upon reasonable request.

Keywords: Activated Carbon · Glycols · Hydrogenolysis · N-doping · Ruthenium

[1] A. N. Marchesan, M. P. Oncken, R. Maciel Filho, M. R. Wolf Maciel, *Green Chem.* **2019**, *21*, 5168–5194.
[2] C. Mondelli, G. Gözaydın, N. Yan, J. Pérez-Ramírez, *Chem. Soc. Rev.* **2020**, *49*, 3764–3782.
[3] Q. Xia, X. Jin, G. Zhang, M. Liu, J. Wang, Y. Li, T. Fang, J. Ding, D. Zhang, K. Meng, X. Chen, C. Yang, *The Chemical Record* **2021**, *21*, 133–148.
[4] C. Montassier, D. Giraud, J. Barbier, in: *Studies in Surface Science and Catalysis, Vol. 41* (Eds.: M. Guisnet, J. Barrault, C. Bouchoule, D. Duprez, C. Montassier, G. Pérot), Elsevier, **1988**, pp. 165–170.

[5] K. Wang, M. C. Hawley, T. D. Furney, *Ind. Eng. Chem. Res.* **1995**, *34*, 3766–3770.
[6] P. J. C. Hausoul, L. Negahdar, K. Schute, R. Palkovits, *ChemSusChem* **2015**, *8*, 3323–3330.
[7] K. L. Deutsch, D. G. Lahr, B. H. Shanks, *Green Chem.* **2012**, *14*, 1635–1642.
[8] J. Sun, H. Liu, *Green Chem.* **2011**, *13*, 135–142.
[9] Z. Tan, L. Shi, Y. Zan, G. Miao, S. Li, L. Kong, S. Li, Y. Sun, *Appl. Catal. A* **2018**, *560*, 28–36.
[10] F. Auneau, M. Berchu, G. Aubert, C. Pinel, M. Besson, D. Todaro, M. Bernardi, T. Ponsetti, R. Di Felice, *Catal. Today* **2014**, *234*, 100–106:.
[11] X. Wang, A. K. Beine, P. J. C. Hausoul, R. Palkovits, *ChemCatChem* **2019**, *11*, 4123–4129.
[12] C. Heisig, C. Glotzbach, S. Schirrmeister, T. Turek, *Chem. Eng. Technol.* **2021**, *44*, 761–772.
[13] P. Yazdani, B. Wang, S. Rimaz, S. Kawi, A. Borgna, *Molecular Catalysis* **2019**, *466*, 138–145.
[14] C. Cai, H. Wang, H. Xin, C. Zhu, Q. Zhang, X. Zhang, C. Wang, Q. Liu, L. Ma, *RSC Adv.* **2020**, *10*, 3993–4001.
[15] J. Pang, M. Zheng, X. Li, Y. Jiang, Y. Zhao, A. Wang, J. Wang, X. Wang, T. Zhang, *Appl. Catal. B* **2018**, *239*, 300–308.
[16] L. S. Ribeiro, N. Rey-Raap, J. L. Figueiredo, J. J. Melo Órfão, M. F. R. Pereira, *Cellulose* **2019**, *26*, 7337–7353.
[17] Z. Xiao, Q. Zhang, T. Chen, C. Cai, Q. Ge, Y. Nie, J. Ji, J. Mao, *Catal. Lett.* **2018**, *148*, 3757–3770.
[18] Y. Jia, Q. Sun, H. Liu, *Appl. Catal. A* **2020**, *603*, 117770.
[19] X. Jin, W. Zhang, D. Zhang, B. Yin, X. Liu, G. Zhang, H. Yan, M. Liu, C. Yang, B. Subramaniam, R. V. Chaudhari, *Materials Today Sustainability* **2020**, *10*, 100047.
[20] P. Kumar, A. K. Shah, J.-H. Lee, Y. H. Park, U. L. Štangar, *Ind. Eng. Chem. Res.* **2020**, *59*, 6506–6516.
[21] S. Li, Y. Zan, Y. Sun, Z. Tan, G. Miao, L. Z. Kong, Y. Sun, *J. Energy Chem.* **2019**, *28*, 101–106.
[22] M. Mounguengui-Diallo, A. Sadier, E. Noly, D. Da Silva Perez, C. Pinel, N. Perret, M. Besson, *Catalysts* **2019**, *9*, 740.
[23] Q. Xia, G. Zhang, J. Wang, W. Zhang, M. Liu, Y. Li, B. Yin, C. Yang, J. Shen, X. Jin, *Ind. Eng. Chem. Res.* **2020**, *59*, 13879–13891.
[24] B. Yin, X. Jin, G. Zhang, H. Yan, W. Zhang, X. Liu, M. Liu, C. Yang, J. Shen, *ACS Sustainable Chem. Eng.* **2020**, *8*, 5305–5316.
[25] M. Zheng, J. Pang, R. Sun, A. Wang, T. Zhang, *ACS Catal.* **2017**, *7*, 1939–1954.
[26] P. J. C. Hausoul, A. K. Beine, L. Neghadar, R. Palkovits, *Catalysis Science, Technology* **2017**, *7*, 56–63.
[27] E. García-Bordejé, in *Heterogeneous Catalysts*, **2021**, pp. 57–77.
[28] A. K. Beine, A. J. D. Krüger, J. Artz, C. Weidenthaler, C. Glotzbach, P. J. C. Hausoul, R. Palkovits, *Green Chem.* **2018**, *20*, 1316–1322.
[29] M. Rivière, N. Perret, A. Cabiac, D. Delcroix, C. Pinel, M. Besson, *ChemCatChem* **2017**, *9*, 2145–2159.
[30] M. Rivière, N. Perret, D. Delcroix, A. Cabiac, C. Pinel, M. Besson, *ACS Sustainable Chemistry & Engineering* **2018**, *6*, 4076–4085; Engineering **2018**, 6, 4076–4085.
[31] L. S. Ribeiro, J. J. M. Órfão, M. F. R. Pereira, *Bioresour. Technol.* **2018**, *263*, 402–409.
[32] X. Jin, P. S. Thapa, B. Subramaniam, R. V. Chaudhari, *ACS Sustainable Chem. Eng.* **2016**, *4*, 6037–6047.
[33] L. Zhao, J. H. Zhou, Z. J. Sui, X. G. Zhou, *Chem. Eng. Sci.* **2010**, *65*, 30–35.
[34] X. Guo, J. Guan, B. Li, X. Wang, X. Mu, H. Liu, *Sci. Rep.* **2015**, *5*, 16451.
[35] C. Montassier, J. C. Ménézo, L. C. Hoang, C. Renaud, J. Barbier, *J. Mol. Catal.* **1991**, *70*, 99–110.
[36] S. Tronci, B. Pittau, *RSC Adv.* **2015**, *5*, 23086–23093.
[37] X. Guo, H. Dong, B. Li, L. Dong, X. Mu, X. Chen, *J. Mol. Catal. A* **2017**, *426*, 79–87.
[38] P. Kuhn, M. Antonietti, A. Thomas, *Angew. Chem.* **2008**, *120*, 3499–3502; *Angew. Chem. Int. Ed.* **2008**, *47*, 3450–3453.
[39] J. Artz, *ChemCatChem* **2018**, *10*, 1753–1771.
[40] M. Liu, L. Guo, S. Jin, B. Tan, *J. Mater. Chem. A* **2019**, *7*, 5153–5172.
[41] C. Krishnaraj, H. S. Jena, K. Leus, P. Van Der Voort, *Green Chem.* **2020**, *22*, 1038–1071.
[42] Z. Qian, Z. J. Wang, K. A. I. Zhang, *Chem. Mater.* **2021**, *33*, 1909–1926.
[43] G. H. Gunasekar, S. Yoon, in: *Emerging Carbon Materials for Catalysis* (Ed.: S. Sadjadi), Elsevier, **2021**, pp. 1–32.
[44] A. Iemhoff, J. Deischter, S. Jung, G. Tuci, G. Giambastiani, R. Palkovits, *J. Mater. Chem. A* **2021**, *9*, 5390–5403.
[45] H. N. T. Le, H. K. Jeong, *New Physics: Sae Mulli* **2015**, *65*, 86–89.
[46] B. Zhang, Z. Wen, S. Ci, S. Mao, J. Chen, Z. He, *ACS Appl. Mater. Interfaces* **2014**, *6*, 7464–7470.
[47] P. Zhang, Q.-N. Wang, X. Yang, D. Wang, W.-C. Li, Y. Zheng, M. Chen, A.-H. Lu, *ChemCatChem* **2017**, *9*, 505–510.
[48] F. Cheng, W.-C. Li, J.-N. Zhu, W.-P. Zhang, A.-H. Lu, *Nano Energy* **2016**, *19*, 486–494.
[49] C. Galeano, J. C. Meier, M. Soorholtz, H. Bongard, C. Baldizzone, K. J. J. Mayrhofer, F. Schüth, *ACS Catal.* **2014**, *4*, 3856–3868.
[50] B. He, W.-C. Li, A.-H. Lu, *J. Mater. Chem. A* **2015**, *3*, 579–585.
[51] R. Arrigo, M. Hävecker, S. Wrabetz, R. Blume, M. Lerch, J. McGregor, E. P. J. Parrott, J. A. Zeitler, L. F. Gladden, A. Knop-Gericke, R. Schlögl, D. S. Su, *J. Am. Chem. Soc.* **2010**, *132*, 9616–9630.
[52] M. Oschatz, J. P. Hofmann, T. W. van Deelen, W. S. Lamme, N. A. Krans, E. J. M. Hensen, K. P. de Jong, *ChemCatChem* **2017**, *9*, 620–628.
[53] R. Hunger, W. Jaegermann, A. Merson, Y. Shapira, C. Pettenkofer, J. Rappich, *J. Phys. Chem. B* **2006**, *110*, 15432–15441.
[54] J. F. Moulder, W. F. Stickle, P. E. Sobol, K. D. Bomben, *Handbook of X-ray Photoelectron Spectroscopy*, Physical Electronics Division, Perkin-Elmer Corporation, **1992**.

Manuscript received: December 15, 2021
Revised manuscript received: March 10, 2022
Accepted manuscript online: March 11, 2022
Version of record online: April 5, 2022